Cellular and Molecular Life Sciences (2020) 77:751–764
https://doi.org/10.1007/s00018-019-03207-0

ORIGINAL ARTICLE

Degranulation of human cytotoxic lymphocytes is a major source of proteolytically active soluble CD26/DPP4

Marcus Lettau[1] · Michelle Dietz[1] · Sarah Vollmers[1] · Fred Armbrust[1] · Christian Peters[1] · Thi Mai Dang[1] · Guranda Chitadze[2] · Dieter Kabelitz[1] · Ottmar Janssen[1]

Received: 12 February 2019 / Revised: 14 June 2019 / Accepted: 24 June 2019 / Published online: 12 July 2019

Abstract

Dipeptidyl peptidase 4 (DPP4, CD26) is a serine protease detected on several immune cells and on epithelial cells of various organs. Besides the membrane-bound enzyme, a catalytically active soluble form (sCD26/DPP4) is detected in several body fluids. Both variants cleave off dipeptides from the N-termini of various chemokines, neuropeptides, and hormones. CD26/DPP4 plays a fundamental role in the regulation of blood glucose levels by inactivating insulinotropic incretins and CD26/DPP4 inhibitors are thus routinely used in diabetes mellitus type 2 therapy to improve glucose tolerance. Such inhibitors might also prevent the CD26/DPP4-mediated inactivation of the T-cell chemoattractant CXCL10 released by certain tumors and thus improve anti-tumor immunity and immunotherapy. Despite its implication in the regulation of many (patho-)physiological processes and its consideration as a biomarker and therapeutic target, the cellular source of sCD26/DPP4 remains highly debated and mechanisms of its release are so far unknown. In line with recent reports that activated T lymphocytes could be a major source of sCD26/DPP4, we now demonstrate that CD26/DPP4 is stored in secretory granules of several major human cytotoxic lymphocyte populations and co-localizes with effector proteins such as granzymes, perforin, and granulysin. Upon stimulation, vesicular CD26/DPP4 is rapidly translocated to the cell surface in a Ca^{2+}-dependent manner. Importantly, activation-induced degranulation leads to a massive release of proteolytically active sCD26/DPP4. Since activated effector lymphocytes serve as a major source of sCD26/DPP4, these results might explain the observed disease-associated alterations of sCD26/DPP4 serum levels and also indicate a so far unknown role of CD26/DPP4 in lymphocyte-mediated cytotoxicity.

Keywords CD26 · Dipeptidylpeptidase 4 · Secretory granules · T cells · NK cells · Lymphocyte-mediated cytotoxicity

Introduction

CD26/Dipeptidylpeptidase 4 (DPP4) is a 110 kDa type 2 transmembrane glycoprotein that belongs to the S9 protease family of prolyl oligopeptidases (EC 3.4.14.5) [1]. As a T-cell surface molecule, CD26/DPP4 has been implicated in the modulation of T-cell activation and proliferation [2]. According to a current model, CD26/DPP4 on T cells interacts with caveolin-1 on antigen-presenting cells and thereby induces an increase in CD86 expression to facilitate T-cell co-stimulation [3]. Simultaneously, caveolin-1-mediated CD26/DPP4-ligation induces T-cell proliferation and NF-κB activation in a TCR/CD3-dependent manner. This is associated with the recruitment of a complex consisting of CD26/DPP4, CARMA1, Bcl10, and IκB kinase to lipid rafts [4]. Consequently, the blockade of the Caveolin-1-CD26/DPP4 interaction with a soluble caveolin-1-Ig fusion protein induces anergy in $CD4^+$ T cells [5]. Moreover, CD26/DPP4-mediated co-stimulation of anti-CD3-activated $CD8^+$ T cells enhances the cytotoxic potential compared to CD28-stimulated T cells [6].

As a serine protease, CD26/DPP4 cleaves off N-terminal dipeptides with penultimate prolines or alanines. Notably, a catalytically active soluble form of CD26/DPP4 (sCD26/

Electronic supplementary material The online version of this article (https://doi.org/10.1007/s00018-019-03207-0) contains supplementary material, which is available to authorized users.

✉ Marcus Lettau
Marcus.Lettau@uksh.de

[1] Institute of Immunology, Christian-Albrechts University Kiel and University Hospital Schleswig-Holstein, Arnold-Heller-Str. 3, Bldg. 17, 24105 Kiel, Germany

[2] Medical Department II, Unit for Hematological Diagnostics, University Hospital Schleswig-Holstein, Langer Segen 8-10, 24105 Kiel, Germany

DPP4) lacking the intracellular and transmembrane domain can be liberated from the plasma membrane [7] and sCD26/DPP4 is detected in serum, saliva, cerebrospinal and seminal fluid, and bile [8]. Importantly, enzymatic DPP4 activity in serum has been mainly attributed to sCD26/DPP4 [7]. CD26/DPP4 substrates include a wide range of gastrointestinal hormones, growth factors, chemokines, neuropeptides, and regulatory peptides. Functional effects of CD26/DPP4-mediated cleavage are quite diverse and include the modulation of receptor specificities, the inactivation of substrates or the generation of bioactive peptides. Described CD26/DPP4 substrates include NPY (neuropeptide Y), GIP (glucose dependent insulinotropic polypeptide), GLP-1/2 (glucagon-like peptide 1/2), CXCL12 (SDF1α, stromal cell-derived factor 1α), Eotaxin, Erythropoietin, GM-CSF (granulocyte macrophage colony-stimulating factor), CXCL10 and CCL5, and many others. This highlights the diversity of biological processes that are modulated by CD26/DPP4 activity (reviewed in [9]) and explains why alterations of sCD26/DPP4 levels and/or activity in serum have been associated with numerous diseases including autoimmunity and cancer [8, 10].

In addition, CD26/DPP4 plays a fundamental role in the systemic regulation of blood glucose levels, since it cleaves and inactivates the insulinotropic incretins GIP and GLP-1. These incretins are released upon glucose intake and enhance insulin secretion. However, their half-life is limited to only a few minutes by the proteolytic activity of CD26/DPP4. Inhibition of CD26/DPP4 prolongs the incretin effect and improves glucose tolerance. Thus, long-term inhibition of CD26/DPP4 has been established as an accompanying therapy in the treatment of diabetes mellitus type 2 (T2DM) and currently 9 DPP4 inhibitors are commercially available that usually reduce DPP4 activity to about 70–90% of baseline level [11]. Despite an overall favorable adverse side-effect profile, concerns of a long-lasting DPP4 inhibition have been put forward after 25 years of treatment, especially with respect to cardiovascular events [12], an increase of infections [13], pancreatitis [14] and even an increased risk for site-specific cancer [15]. These long-term treatment-associated events highlight that a deeper insight into CD26/DPP4 functions in- and outside the immune system is urgently needed.

Surprisingly, despite the suggested prognostic value of sCD26/DPP4 as a serum marker in multiple diseases, its fundamental role in blood glucose level regulation and as a major drug target in diabetes type 2 therapy, the cellular source of sCD26/DPP4 remains highly debated. CD26/DPP4 is rather ubiquitously expressed on blood cells, fibroblasts, mesothelial, epithelial, and endothelial cells and is detected in several organs including placenta, kidney, intestine, prostate, gall bladder, pancreas, and liver [16–18]. In the immune system, CD26/DPP4 is expressed on dendritic cells, activated B cells, NK cells, T cells, and $CD34^+$ progenitor cells (reviewed in [1]). Here, CD26/DPP4 surface expression was suggested as a marker to evaluate the effector/memory state of $CD8^+$ T cells [6], the suitability of $CD4^+$ T cells for cancer immunotherapy [19], and the haematopoietic recovery and lymphocyte reconstitution after autologous hematopoietic stem-cell transplantation in multiple myeloma patients [20]. With respect to the cellular source of sCD26/DPP4, recent in vivo studies in mice suggested that both endothelial and bone-marrow-derived cells contribute to sCD26/DPP4 serum levels and activity [21]. Based on the notion that SCID patients and mice display reduced plasma levels of sCD26/DPP4, Casrouge and colleagues provided further correlative experimental evidence that sCD26/DPP4 plasma concentrations and activity depend on the abundance and activation state of T lymphocytes [22].

We had previously noted that CD26/DPP4 is stored in different secretory granules of in vitro expanded T-cell blasts [23, 24]. With a focus on cytotoxic lymphocytes, we now demonstrate that upon stimulation or target cell encounter, CD26/DPP4 is rapidly translocated to the cell surface in a Ca^{2+}-dependent manner. Moreover, activation-induced degranulation leads to a massive release of proteolytically active sCD26/DPP4. Thus, we propose that indeed, activated cytotoxic lymphocytes (CL) serve as a major source of sCD26/DPP4 and that degranulation mechanistically governs sCD26/DPP4 release.

Results

Performing proteomic profiling of lysosome-related effector vesicles of human T cells, we identified CD26/DPP4 as a cargo protein of T-cell granules [23, 24]. To analyze the subcellular localization of CD26/DPP4 in more detail, freshly isolated peripheral blood mononuclear cells (PBMC) were permeabilized, stained with fluorophore-conjugated anti-CD4 or anti-CD8 and anti-CD26/DPP4 antibodies, and analyzed via imaging flow cytometry (Fig. 1/Sup. Fig. 1). The $CD8^+$ compartment segregated into cells with high or low expression of CD8 referred to as $CD8^{high}$ and $CD8^{low}$ cells, respectively (Sup. Fig. 1E). In permeabilized lymphocytes, CD26/DPP4 is located in intracellular granules in both $CD4^+$ and $CD8^+$ cells (Fig. 1a). This phenotype is characterized by a high bright detail intensity (BDI) of the CD26/DPP4 staining. The BDI feature computes the intensity of localized bright spots within the masked area in a given image while removing the local background surrounding the spots before intensity calculation. Thus, plotting of the fluorescence intensity (FI) against the BDI of the CD26/DPP4 staining allows for the identification of cells with granular localization of CD26/DPP4 (termed $CD26/DPP4^{intra}$ cells in the following, Fig. 1b). Although the fluorescence intensity already

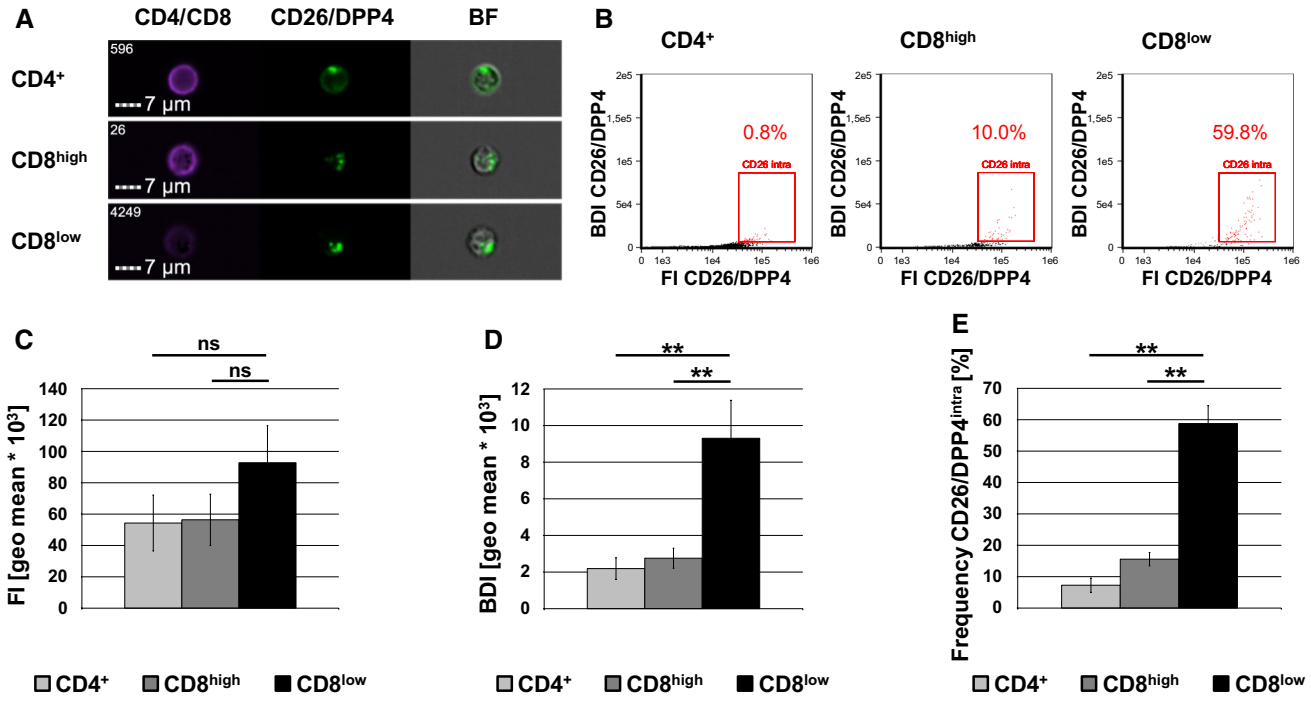

Fig. 1 Subcellular localization of CD26/DPP4 in $CD4^+$ and $CD8^+$ lymphocytes. Freshly isolated PBMC derived from five healthy blood donors were stained with a LIVE/DEAD™ Fixable Far Red Dead Cell Stain, fixed, permeabilized and stained with Brilliant Violet 421-conjugated anti-CD4 (clone OKT4) or anti-CD8 mab (clone RPA-T8) and FITC-conjugated anti-CD26/DPP4 mab (clone BA5b) or an appropriate isotype control. 10.000 cells were acquired with an ImageStream Mark II imaging cytometer. Only focused, single, viable $CD4^+$ or $CD8^+$ cells were considered for further analyses. **a** Representative images of $CD4^+$ (upper panel), $CD8^{high}$ (middle panel) and $CD8^{low}$ (lower panel) lymphocytes (BF, brightfield). Scale bars represent 7 µm. **b** Dot plot analysis of the fluorescence intensity (FI) and the bright detail intensity (BDI) of the CD26/DPP4 staining (black dots) displaying the percentage of $CD4^+$, $CD8^{high}$ and $CD8^{low}$ lymphocytes with a high CD26/DPP4 FI and BDI ($CD26/DPP4^{intra}$, red dots). Cells stained with isotype control antibodies are displayed as grey dots. **c** Fluorescence intensity of the CD26/DPP4 staining. **d** Bright detail intensity of the CD26/DPP4 staining. **e** Frequency of $CD26/DPP4^{intra}$ cells among $CD4^+$, $CD8^{high}$ and $CD8^{low}$ cells. Data are displayed as mean values of experiments with cells derived from five independent healthy blood donors ± SEM. Statistical significance between different subpopulations is displayed as ** for $p < 0.01$ (Mann–Whitney *U* test); *ns* not significant

revealed a difference in CD26/DPP4 expression between $CD4^+$ and $CD8^{low}$ cells as well as between $CD8^{high}$ and $CD8^{low}$ cells (Fig. 1c), those differences become statistically significant when calculating the BDI (Fig. 1d). Applying both features to assess the frequency of $CD26/DPP4^{intra}$ cells revealed that 7% of $CD4^+$ lymphocytes store CD26/DPP4 in intracellular granules, whereas 16% of the freshly isolated $CD8^{high}$ cells showed an intracellular/granular expression of CD26/DPP4, although the observed difference did not show significance among the five included donors. However, 59% of $CD8^{low}$ cells exhibited intracellular/granular CD26/DPP4 expression and this increased frequency of $CD26/DPP4^{intra}$ cells is significant when compared to $CD4^+$ or $CD8^{high}$ cells of the same cohort of donors (Fig. 1e). Since NK cells have been shown to frequently express CD8 at low levels, we assessed the frequency of $CD56^+$ within the $CD8^{high}$ and $CD8^{low}$ populations (Sup. Fig. 2A). These analyses revealed that only few $CD8^{high}$ cells, but 74% of $CD8^{low}$ cells express CD56 indicating that this population might comprise NK cells, although also NKT and some $CD8^+$ T cells express CD56 [25].

As mentioned, we identified CD26/DPP4 as a cargo protein of lysosome-related effector vesicles (LREV) that were also characterized by a high abundance of cytotoxic effector proteins. It is well established that soluble cytotoxic effector molecules are safely stored in LREV of CLs to allow for their instant release upon appropriate stimulation [26]. Using freshly isolated PBMC from healthy donors, we thus analyzed the co-localization of intracellular CD26/DPP4 with the cytotoxic effector proteins granzyme (Grz) A, GrzB, perforin (Prf), and granulysin (Gnly) in lymphocytes associated with cytotoxic effector potential including $CD8^+$/TCR $\alpha\beta^+$, $CD3^+$/TCR $\gamma\delta^+$, and $CD3^-/CD56^+$ cells. These analyses revealed that intracellular/granular CD26/DPP4 co-localizes with GrzA (Fig. 2a), GrzB (Fig. 2b), Prf (Fig. 2c) and Gnly (Fig. 2d). Again, the frequency of $CD26/DPP4^{intra}$ cells was most pronounced in $CD3^-/CD56^+$ cells, but also 20–30% of $CD8^+$/TCR $\alpha\beta^+$ and $CD3^+$/TCR $\gamma\delta^+$ cells

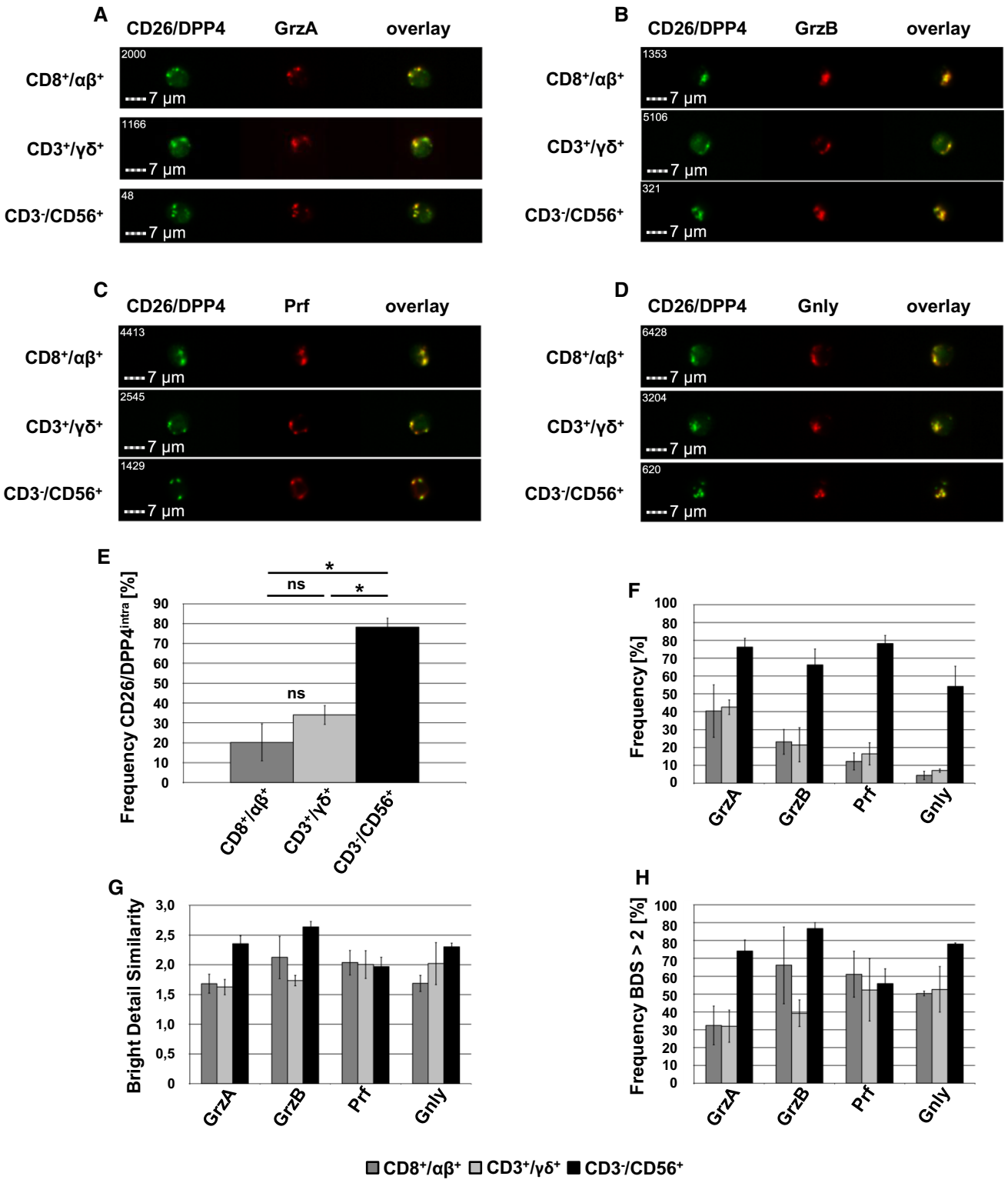

showed intracellular storage of CD26/DPP4 although with notable donor-dependent variability (Fig. 2e). As expected, $CD3^{-}/CD56^{+}$ cells showed the highest frequency of $GrzA^{+}$, $GrzB^{+}$, Prf^{+}, and $Gnly^{+}$ cells that were again identified on the basis of both the FI and the BDI of the respective staining. Expression of cytotoxic effector molecules was less pronounced in $CD8^{+}$/TCR $\alpha\beta^{+}$ and $CD3^{+}$/TCR $\gamma\delta^{+}$ cells and declines in the order GrzA > GrzB > Prf > Gnly (Fig. 2f). Again, we observed considerable donor-dependent variations especially in T cells. We quantified the degree of

◂**Fig. 2** Co-localization of intracellular CD26/DPP4 with the cytotoxic effector proteins granzyme A, granzyme B, perforin and granulysin in freshly isolated PBMC. Freshly isolated PBMC were stained with either Brilliant Violet 421-conjugated anti-CD8 mab (clone RPA-T8) and APC-conjugated anti-TCR αβ mab (clone IP26), Brilliant Violet 421-conjugated anti-CD3 mab (clone UCHT1) and APC-conjugated anti-TCR γδ mab (clone B1) or Brilliant Violet 421-conjugated anti-CD3 mab (clone UCHT1) and APC-conjugated anti-CD56 mab (clone 5.1H11). Following permeabilization, cells were stained with FITC-conjugated anti-CD26/DPP4 mab (clone BA5b) and PE-conjugated anti-GrzA mab (clone CB9) or PE-conjugated anti-GrzB mab (clone GB11), PE-conjugated anti-perforin mab (clone dG9) or PE-conjugated anti-GNLY mab (clone DH2). 10.000 cells were acquired with an ImageStream Mark II imaging cytometer. Only focused, single, $CD8^+$/TCR $\alpha\beta^+$, $CD3^+$/TCR $\gamma\delta^+$ and $CD3^-/CD56^+$ or cells were considered for further analyses. **a**–**d** Representative images of $CD8^+$/TCR $\alpha\beta^+$ (upper panel), $CD3^+$/TCR $\gamma\delta^+$ (middle panel) and $CD3^-/CD56^+$ (lower panel) lymphocytes stained for **a** GrzA, **b** GrzB, **c** Prf and **d** Gnly. Scale bars represent 7 µm. **e** Percentage of $CD8^+$/TCR $\alpha\beta^+$, $CD3^+$/TCR $\gamma\delta^+$ and $CD3^-/CD56^+$ cells with intracellular expression of CD26/DPP4 or **f** GrzA, GrzB, Prf and Gnly. **g** Geometric mean of the bright detail similarity score of the GrzA/CD26/DPP4, GrzB/CD26/DPP4, Prf/CD26/DPP4 and Gnly/CD26/DPP4 staining of $CD8^+$/TCR $\alpha\beta^+$, $CD3^+$/TCR $\gamma\delta^+$ and $CD3^-/CD56^+$ cells. **h** Percentage of $CD8^+$/TCR $\alpha\beta^+$, $CD3^+$/TCR $\gamma\delta^+$ and $CD3^-/CD56^+$ cells displaying a BDS score > 2 of the GrzA/CD26/DPP4, GrzB/CD26/DPP4, Prf/CD26/DPP4 and Gnly/CD26/DPP4 stainings. Data are displayed as mean values of cells derived from three healthy blood donors ± SEM. Statistical significance between different subpopulations is displayed as * for $p < 0.1$ (Mann–Whitney *U* test; *ns* not significant)

co-localization employing the bright detail similarity (BDS) feature, which represents the log-transformed Pearson correlation of respective images on a pixel-by-pixel and cell-by-cell basis [27] (Fig. 2g). In $CD8^+$/TCR $\alpha\beta^+$ cells, the mean overall BDS score ranged from 1.7 for the co-localization of intracellular CD26/DPP4 with GrzA and Gnly to 2.0 for Prf and 2.1 for GrzB. In $CD3^+$/TCR $\gamma\delta^+$ cells the mean BDS score for the co-localization of intracellular CD26/DPP4 with GrzA was 1.6, with GrzB 1.7 and with Prf and Gnly 2.0. Again, we observed notable donor-dependent variations. Those variations were less pronounced in $CD3^-/CD56^+$ cells that also showed the highest degree of co-localization of intracellular CD26/DPP4 with GrzA (BDS 2.4), GrzB (BDS 2.6), Prf (BDS 2.0) and Gnly (BDS 2.3). Of note, it is well established that Prf is stored in $CD107^+$ storage granules and the co-localization of Prf with the lysosomal marker protein CD107a results in an overall BDS score of 2.0 in our experimental system [28]. We also calculated the frequency of cells that displayed a BDS score > 2 for the co-localization of cytotoxic effector proteins with granular CD26/DPP4 (Fig. 2h). Among $CD8^+$/TCR $\alpha\beta^+$ cells, 32% of CD26/$DPP4^{intra}$/$GrzA^+$ cells, 66% of CD26/$DPP4^{intra}$/$GrzB^+$ cells, 61% of CD26/$DPP4^{intra}$/Prf^+ cells and 50% of CD26/$DPP4^{intra}$/$Gnly^+$ cells display a BDS score > 2 and among $CD3^+$/TCR $\gamma\delta^+$ cells, 32% of CD26/$DPP4^{intra}$/$GrzA^+$ cells, 39% of CD26/$DPP4^{intra}$/$GrzB^+$ cells, 52% of CD26/$DPP4^{intra}$/Prf^+ cells and 53% of CD26/$DPP4^{intra}$/$Gnly^+$ cells display a BDS score > 2. Again, results for T cells proved to be quite heterogeneous between cells isolated from different blood donors. Among the $CD3^-/CD56^+$ NK cells, 74% of CD26/$DPP4^{intra}$/$GrzA^+$ cells, 87% of CD26/$DPP4^{intra}$/$GrzB^+$ cells, 56% CD26/$DPP4^{intra}$/Prf^+ cells and 78% of CD26/$DPP4^{intra}$/$Gnly^+$ cells display a BDS score > 2. We thus observe a clear although partial co-localization of granular CD26/DPP4 with cytotoxic effector proteins in CLs. However, the degree of co-localization differs between subpopulations and even within a given subpopulation. Especially in the case of T cells, we observed high donor-dependent variability indicating that also the activation state might influence co-localization.

Of note, also $CD3^+$/TCR$\gamma\delta^+$ T cells store considerable amounts of CD26/DPP4 and these cells can be easily activated and expanded by cultivation in the presence of aminobisphosphonates such as zoledronic acid [29]. We thus isolated PBMC from healthy blood donors and expanded γδ T cells with zoledronic acid in the presence of IL-2. Respective cell cultures usually contained ~ 90% γδ T cells after 10–14 days of expansion. In a first step, we analyzed the expression and subcellular localization of CD26/DPP4 and cytotoxic effector molecules as we did before in freshly isolated cells. After activation and expansion, 68% of $CD3^+$/TCR $\gamma\delta^+$ expressed GrzA, 50% GrzB, 35% Prf, 39% Gnly, and 78% intracellular CD26/DPP4 (Fig. 3a). As evident from the overall BDS score (Fig. 3b) and the frequency of cells displaying a BDS score > 2 (Fig. 3c), we again observed a high degree of co-localization of intracellular CD26/DPP4 with cytotoxic effector molecules.

In a next step, we aimed to biochemically verify the storage of CD26/DPP4 in lysosome-related effector vesicles. We thus homogenized zoledronate-expanded γδ T cells, enriched the organelles as previously described [30], and separated the material by ultracentrifugation on a discontinuous iodixanol gradient. Interestingly, in γ/δ T cells and NK cells CD26/DPP4 was more abundant in enriched organelles (Fig. 3d) and especially in the crude lysosomal fractions (Fig. 3d, f) when compared to the cytosolic fraction. This differential abundance was, however, less prominent for the $CD8^+$ T-cell preparation, as depicted in Fig. 3e. Notably, several organelle fractions are also characterized by the presence of CD107a indicative of lysosomal storage granules. Of note, CD26/DPP4 is present in the $GrzB^+$ heavy fraction although it shows a broader distribution (Fig. 3d). Besides $CD3^+$/TCR$\gamma\delta^+$ T cells, also $CD8^+$/TCR $\alpha\beta^+$ cells store considerable amounts of CD26/DPP4. We thus MACS-sorted $CD8^+$ T cells from PBMC of healthy donors and stimulated the cells with a cocktail of irradiated allogeneic PBMC and EBV-transformed lymphoblastoid B cells in the presence of phytohemagglutinin (PHA) and IL-2. After expansion, $CD8^+$ T cells were subjected

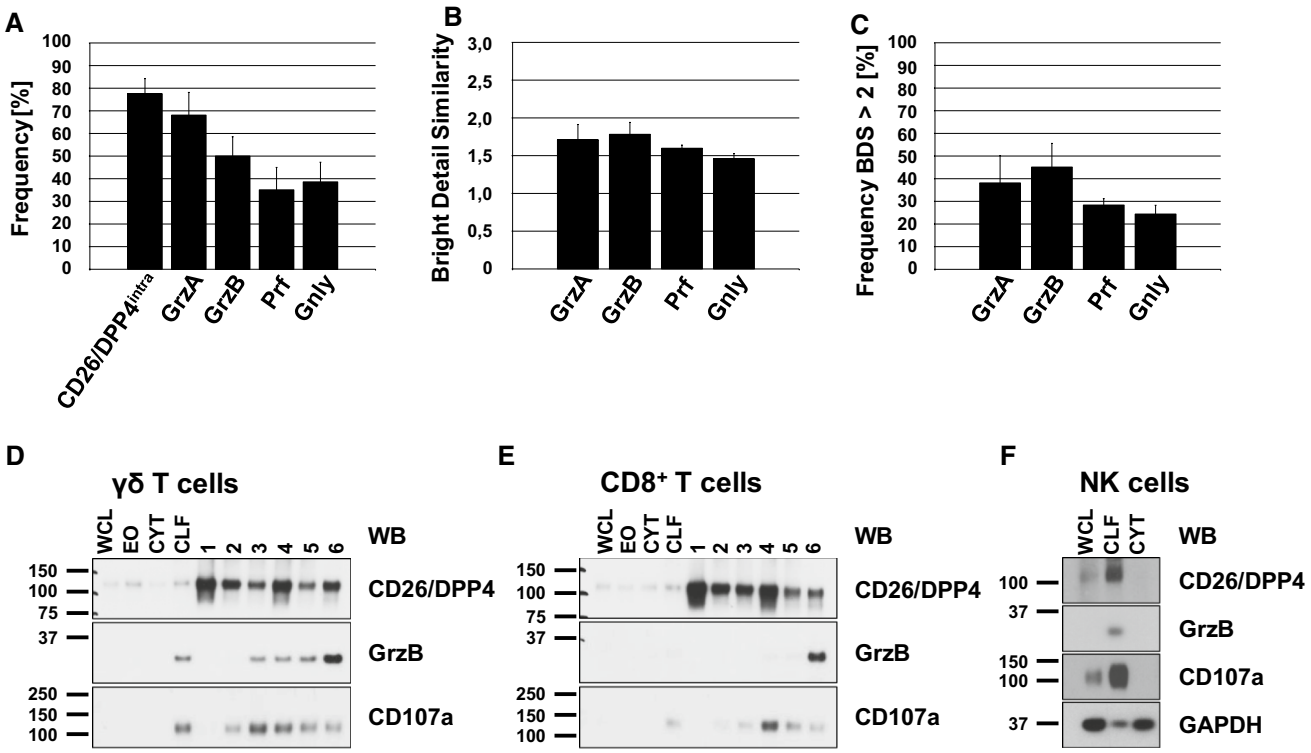

Fig. 3 Intracellular storage of CD26/DPP4 in expanded T-cell lines. PBMC were incubated with zoledronic acid and expanded in the presence of IL-2. Cells were stained with Brilliant Violet 421-conjugated anti-CD3 mab (clone UCHT1) and APC-conjugated anti-TCR γδ mab (clone B1), permeabilized and stained with FITC-conjugated anti-CD26/DPP4 mab (clone BA5b) and PE-conjugated anti-GrzA mab (clone CB9), PE-conjugated anti-GrzB mab (clone GB11), PE-conjugated anti-perforin mab (clone dG9) or PE-conjugated anti-Gnly mab (clone DH2). 10.000 cells were acquired with an ImageStream Mark II imaging cytometer. Only focused, single, $CD3^+$/TCR $\gamma\delta^+$ cells were considered for further analyses. **a** Percentage of $CD3^+$/TCR $\gamma\delta^+$ cells expressing GrzA, GrzB, Prf, Gnly and intracellular CD26/DPP4. **b** Geometric mean of the bright detail similarity score of the GrzA/CD26/DPP4, GrzB/CD26/DPP4, Prf/CD26/DPP4 and Gnly/CD26/DPP4 staining of expanded γδ T cells. **c** Percentage of γδ T cells displaying a BDS score > 2 of the GrzA/CD26/DPP4, GrzB/CD26/DPP4, Prf/CD26/DPP4 and Gnly/CD26/DPP4 stainings. Data are displayed as mean values of cells derived from three healthy blood donors ± SEM. **d** Zoledronate-activated γδ T cells and **e** MACS-purified $CD8^+$ T cells were expanded for 14 days, homogenized and organelle extraction and separation were performed as described. Equal amounts of protein from whole cell lysates (WCL), enriched organelles (EO), cytosol (CYT) and crude lysosomal fraction (CLF) and the individual fractions 1–6 obtained after density gradient ultracentrifugation were separated by SDS-PAGE and transferred to nitrocellulose. Western blots were stained for CD26/DPP4, GrzB and CD107a and are representative for 3 independent experiments. **f** MACS-purified NK cells were expanded for 16 days, homogenized and organelle extraction and separation were performed as described. Equal amounts of protein from whole cell lysate (WCL), the crude lysosomal fraction (CLF) and the cytosol (CYT) were separated by SDS-PAGE, transferred to nitrocellulose and Western blots were stained for CD26/DPP4, GrzB, CD107a and GAPDH

to the enrichment of lysosome-related effector vesicles as described before. As observed for expanded γδ T cells, CD26/DPP4 is highly abundant in $CD107a^+$ fractions and also present in the $GrzB^+$ heavy fraction (Fig. 3e). Moreover, MACS-purified and in vitro expanded NK cells were also subjected to subcellular fractionation, although density gradient centrifugation of the crude lysosomal fraction was not performed due to lower cell numbers. Nevertheless, both CD26/DPP4 and GrzB are clearly enriched in the $CD107^+$ lysosomal fraction compared to the whole cell lysate or the cytosolic fraction (Fig. 3f).

Upon target cell encounter, secretory granules are transported to the site of intercellular contact, where they fuse with the plasma membrane to release the soluble effector molecules into the immunological synapse and to expose transmembrane proteins locally on the cell surface. To address the inducible mobilization of CD26/DPP4, γδ T cells were stimulated with a combination of the agonistic anti-CD3 mab OKT3 and a cross-linking rabbit anti-mouse antibody. We followed the kinetics of CD26/DPP4 surface expression by flow cytometry for up to 3 h (Fig. 4a). Upon CD3 ligation, CD26/DPP4 is mobilized to the cell surface after only 20 min. With ongoing stimulation, CD26/DPP4 surface expression remains increased compared to unstimulated cells. Classical degranulation including GrzB release and CD107a surface exposure strictly depends on calcium signaling [28]. We thus tested whether Ca^{2+} chelation by EGTA modulates activation-induced CD26/DPP4 surface

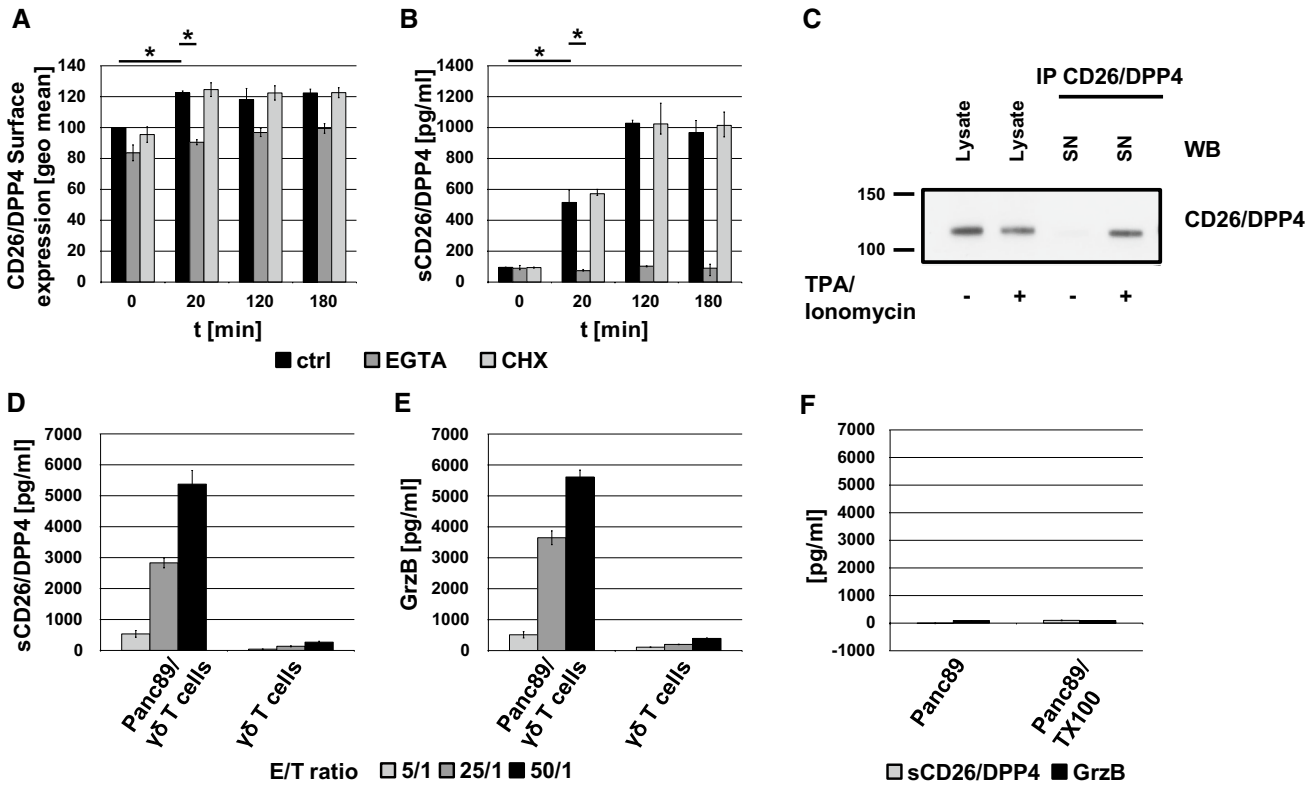

Fig. 4 Activation-induced mobilization of (s)CD26/DPP4 from γδ T cells. **a**, **b** Zoledronate-expanded γδ T cells were stimulated with anti-CD3 mab OKT3 (1 µg/mL) and cross-linking rabbit anti-mouse IgG (1.2 µg/mL) for up to 3 h in the presence of 4 mM EGTA and 4 mM $MgCl_2$ (dark grey bars), 1 µM Cycloheximide (CHX, light grey bars) or without further additions (black bars). **a** Cells were stained with an FITC-conjugated anti-CD26/DPP4 mab (clone BA5b) and surface expression was determined by flow cytometry. Geometric mean fluorescence intensities of unstimulated cells in the absence of inhibitor were set to 100%. **b** Amount of sCD26/DPP4 in cellular supernatants was determined by ELISA. Data are displayed as mean values of 3 single experiments ± SD. Statistical significance between unstimulated and stimulated cells and cells treated with EGTA or not is displayed as * for $p < 0.1$ (Mann–Whitney *U* test). **c** Zoledronate-expanded γδ T cells were either stimulated with phorbol ester (TPA, 20 ng/mL) and calcium ionophore (ionomycin, 500 ng/mL) for 2 h or left untreated. CD26/DPP4 was precipitated from cell-free supernatants of unstimulated and stimulated cells with anti-CD26/DPP4 mab 202.36. Equal amounts of protein from NP40 lysates of unstimulated and stimulated cells and respective precipitates were separated by SDS-PAGE, transferred to nitrocellulose and CD26/DPP4 was detected by immunoblot with anti-CD26/DPP4 mab D6D8K. This experiment is representative for three independent experiments. **d, e** Zoledronate-expanded γδ T cells were incubated with Panc89 tumor cells in the presence of additional BrHPP (300 nM) and IL-2 (50 U/ml) at effector/target (E/T) ratios of 5/1 (light grey), 25/1 (dark grey) and 50/1 (black) or were left untreated. After 4 h at 37 °C, cell-free supernatants were harvested and the amount of released sCD26/DPP4 (**d**) and GrzB (**e**) was assessed by ELISA. **f** As a control, the amount of sCD26/DPP4 and GrzB released from Panc98 cells after lysis with Triton X-100 (TX100) or without treatment was also determined. Data are displayed as mean values of 3 single experiments ± SD

expression. Interestingly, CD26/DPP4 surface mobilization is completely abrogated in the presence of EGTA. Moreover, pre-incubation of cells with the translation inhibitor cycloheximide did not influence surface expression levels of CD26/DPP4, indicating that the observed increase relies on the mobilization of pre-stored molecules.

However, since the activation-induced increase of CD26/DPP4 surface expression was rather moderate, we assessed whether γδ T cells might also release soluble sCD26/DPP4 upon stimulation. We thus tested supernatants of CD3-stimulated γδ T cells for the presence of sCD26/DPP4 by ELISA. Indeed, we observed a substantial release of sCD26/DPP4 into the supernatant upon CD3 ligation after only 20 min of stimulation. Ongoing stimulation further elevated sCD26/DPP4 levels. This release was completely abolished in the presence of EGTA, whereas cycloheximide pre-treatment of the cells had no effect (Fig. 4b). Of note, comparable kinetics of the activation-induced surface expression and release of (s)CD26/DPP4 were also observed with activated and in vitro expanded $CD8^+$ T cells (Sup. Fig. 2B/C). Analyses of respective supernatants with a fluorogenic DPP4 protease activity assay revealed that sCD26/DPP4 released by γδ T cells is proteolytically active and reaches activity levels in the range of serum levels of a healthy individuum used as a control (Sup. Fig. 2d). To biochemically prove the activation-dependent release of sCD26/DPP4, we precipitated

the molecule from supernatants of stimulated cells (Fig. 4c). To avoid interference of anti-CD3 antibodies with immunoprecipitation, cells were stimulated with phorbolester and calcium ionophore to mimic TCR signaling. Only upon activation, sCD26/DPP4 was precipitated from supernatants of stimulated cells. Moreover, the released sCD26/DPP4 migrated slightly below cellular CD26/DPP4 which might be indicative of a potential proteolytic cleavage prior to its release.

We then sought to assess the release of sCD26/DPP4 in an effector/target cell situation. It is well established that γδ T-cell lyse pancreatic ductal adenocarcinoma (PDAC) cells in the presence of phosphoantigens (pAg) [31]. Therefore, we incubated zoledronate-expanded γδ T cells with the PDAC cell line Panc89 in the presence of the pAg BrHPP at different effector/target ratios (50/1, 25/1, 5/1). Interestingly, upon co-culture with tumor target cells, effector lymphocytes release high amounts of sCD26/DPP4 (Fig. 4d) and the cytotoxic effector protein GrzB (Fig. 4e), whereas hardly any constitutive release is observed. Of note, we did not detect sCD26/DPP4 or GrzB in supernatants of Panc89 cells in the absence of effector cells or of Panc89 cells lysed with Triton X-100 (Fig. 4f). Thus, also target cell elimination is clearly associated with the release of sCD26/DPP4 from effector cells.

Discussion

We detected pre-stored CD26/DPP4 in intracellular granules of $CD4^+$ and $CD8^+$ αβ T cells, of γδ T cells and of NK cells. Co-localization analyses of CD26/DPP4 with soluble cytotoxic effector proteins including GrzA, GrzB, Prf, and Gnly verified the storage in cytotoxic effector granules of respective cells. Of note, bright detail similarity scores were highest in NK cells but overall lower in T cells. Moreover, in the latter case, donor-dependent variations were more pronounced. Nevertheless, also in T cells a fraction of cells displayed an evident co-localization of intracellular CD26/DPP4 with cytotoxic effector proteins. However, although enrichment of different lysosome-related effector vesicles from expanded $CD8^+$ T cells and γδ T cells verified the localization in granzyme B storage compartments, we also noticed a broader distribution of CD26/DPP4. This is in line with immunofluorescence images of individual cells with a low bright detail similarity score of the CD26/DPP4 staining and the staining of cytotoxic effector molecules that might indeed indicate a segregation to different compartments in individual cells. Since the intracellular trafficking of CD26/DPP4 is only poorly understood, this might well reflect transient localization in intermediates of its trafficking pathway. However, we cannot exclude that alternative storage compartments might be employed as well. Since donor-dependent variations in co-localization were most pronounced in peripheral blood T cells, the activation state of the cells might also well influence CD26/DPP4 storage.

In general, CD26/DPP4 is supposed to be mainly located on the cell surface and the subcellular localization has not been analyzed in detail yet. Therefore, even the functional role of CD26/DPP4 within the immune system or its role as a marker and co-stimulatory molecule for T-cell activation might only be one facet of its overall functions. Along this line, there are only very few reports on the intracellular expression of CD26/DPP4. Already in 1990, Fukui and colleagues detected CD26/DPP4 in lysosomes of hepatocytes, endothelial cells, and Kupffer cells in ultrathin sections of rat liver by immunogold electron microscopy [32]. In pancreatic islets of the pig, immunoelectron microscopy revealed the presence of CD26/DPP4 in the secretory granules of A cells [33]. Casey et al. identified CD26/DPP4 in a proteomic screen of enriched organelles from the lymphoblastic leukemia/lymphoma NK-cell line YTS. The organelle fractions obtained after density gradient centrifugation displayed an enrichment of the lysosomal transmembrane protein CD63 and Alpha-N-acetylgalactosaminidase activity in the absence of calnexin, TGN46, EEA1, MPR, and GLUT1 and thus likely represent enriched secretory lysosomes/cytotoxic granules [34]. Interestingly, based on the finding that both $CD26/DPP4^+$ and $CD26/DPP4^-$ T cells exhibit comparable levels of CD26/DPP4 mRNA and overall protein, Mattern and co-workers already suggested an intracellular pool of CD26/DPP4 in T cells [35]. Along this line, we identified CD26/DPP4 as a cargo protein of lysosome-related effector vesicles also in non-transformed human T cells by proteome profiling [23, 24].

We now demonstrate that upon TCR ligation, pre-stored CD26/DPP4 is rapidly mobilized from intracellular storage granules in a strictly calcium-dependent fashion and thus follows the hallmarks of classical degranulation. Interestingly, activation-induced surface expression was rather moderate. Instead, we observed a major release of proteolytically active sCD26/DPP4 into the supernatant. Notably, although fairly high levels of sCD26/DPP4 are detected in diverse body fluids such as serum, saliva, cerebrospinal, and seminal fluid and bile [8], the cellular source of sCD26/DPP4 remains highly controversial despite its fundamental role as a therapeutic target for blood glucose regulation and its apparent prognostic value for a plethora of different diseases. In CD26/DPP4 deficient rats, plasma DPP4 activity was partially restored after reconstitution with wild-type bone marrow, indicating that bone-marrow-derived cells constitute an important source of plasma sCD26/DPP4 [36]. In line with these results, the combined genetic ablation of CD26/DPP4 from endothelial cells and bone-marrow-derived cells in mice significantly reduced total plasma DPP4 activity that was partially restored upon bone-marrow transplantation,

suggesting that both bone-marrow-derived and endothelial cells contribute to plasma sCD26/DPP4 levels [21]. Only recently, Casrouge and co-workers showed that individuals with congenital lymphocyte-immunodeficiency displayed decreased sCD26/DPP4 serum levels that were normalized upon restoration of hematopoiesis [22]. Moreover, sCD26/DPP4 serum levels in healthy controls or treated patients correlated with numbers of circulating lymphocytes. In vitro analyses revealed that T-cell stimulation increased the sCD26/DPP4 release. Along this line, infection of mice with influenza virus resulted in elevated sCD26 serum levels that correlated with an increased frequency of antigen-specific $CD8^+$ T cells [22]. Nargis and co-workers showed that plasma DPP4 activity in Diabetes mellitus type 2 patients is linked to the enhanced release of sCD26/DPP4 from circulating TH17 cells. In this scenario, patient TH17 cells showed reduced surface expression of CD26/DPP4 that positively correlated with increased plasma DPP4 activity arguing for TH17 cells as a source for the elevated plasma CD26/DPP4 abundance associated with T2DM [37]. In addition, adipocytes have also been identified as a source for sCD26/DPP4 [38–40] and hepatocytes also secrete sCD26/DPP4, especially in obese mice [40, 41].

It is generally assumed that sCD26/DPP4 originates from the proteolytic cleavage of full length CD26/DPP4 [37, 39] liberating the proteolytically active soluble form that lacks the intracellular region and the transmembrane domain [7]. However, the protease(s) mediating sCD26/DPP4 release remain(s) to be identified, although the metalloproteases MMP1, MMP2, and MMP14 have been implicated in the liberation of sCD26/DPP4 from smooth muscle cells, MMP14 in the shedding from adipocytes [39] and the serine protease kallikrein 5 (KLK5) in the release from TH17 cells [37]. Of note, in our hands, broadband inhibitors of serine proteases (AEBSF, 4-(2-aminoethyl)benzenesulfonyl fluoride hydrochloride) and metalloproteases (TAPI-1) did not modulate the activation-induced release of sCD26/DPP4 (unpublished data). Importantly, we detected the released sCD26/DPP4 by both immunoprecipitation with subsequent Western blot and ELISA. We observed only a minor difference in the molecular weight of sCD26/DPP4 released into the supernatant and CD26/DPP4 precipitated from cellular lysates. However, given that the soluble form is suggested to comprise amino acids 39-766 [7] and the extracellular portion is heavily glycosylated, only a small difference in the migratory behaviour during electrophoresis is expected. Ultracentrifugation of supernatants prior analysis revealed that putative exosomal/microvesicular CD26/DPP4 does not contribute to levels of sCD26/DPP4 assessed by ELISA (not shown). Of note, besides shedding of transmembrane CD26/DPP4 from the cell surface it might also be processed within intracellular storage granules to allow for the rapid release of sCD26/DPP4 upon mobilization and fusion of cytotoxic granules with the plasma membrane. Poulsen and co-workers previously suggested that CD26/DPP4 is stored in secretory granules of A cells of pancreatic islets as a soluble protein, since immunogold electron microscopy did not reveal a specific association with the granule membrane [33]. Although we did not detect truncated CD26/DPP4 in cellular lysates, an intracellular processing might well be induced by T-cell activation and precede degranulation. However, additional studies are required to assess the cellular site of CD26/DPP4 processing.

sCD26/DPP4 released from cytotoxic lymphocytes upon degranulation is proteolytically active and CD26/DPP4-mediated processing of the incretin hormones GIP and GLP-1/2 accounts for the role of CD26/DPP4 in the regulation of blood glucose levels [11]. However, recent in vivo data suggested that sCD26/DPP4 released by bone-marrow-derived cells controls plasma levels of GIP only and not of GLP-1/2 and might, furthermore, not contribute to glucose control [21]. In this scenario, it might be interesting to evaluate the effect of CD26/DPP4-deficiency in hematopoietic cells on the regulation of blood glucose levels during an immune response to infections, autoimmunity or immunotherapy of cancer malignancies. Further substrates of sCD26/DPP4 include, for example, the chemokines CXCL12 (SDF1α) and CXCL10 (reviewed in [9]). CXCL12 is a highly efficient chemoattractant for lymphocytes, monocytes, and $CD34^+$ hematopoietic precursor cells expressing its receptor CXCR4 and CD26/DPP4-mediated conversion of CXCL12 [1–67] to CXCL12 [3–67] completely abolishes SDF1α chemotactic properties [42], and since CXCL12 [3–67] retains significant binding affinity for the receptor, it antagonizes binding of biologically active CXCL12 [1–67] [43]. In contrast, CD26/DPP4-mediated N-terminal truncation of CXCL10 results in the generation of an antagonist form of the chemokine that limits T-cell and NK-cell migration. Notably, in vivo DPP4 inhibition in humans can preserve the bioactive form of CXCL10 thus opening new perspectives for the use of DPP4 inhibitors as therapeutic immune modulators by affecting T- and NK-cell trafficking [44]. Independent of its enzymatic activity, hepatocyte-derived sCD26/DPP4 was shown to activate macrophages via caveolin-1 ligation and to contribute to obesity-associated inflammation in mice [41]. These few examples already highlight the functional diversity and complexity of the impact of CD26/DPP4-mediated substrate processing and of sCD26/DPP4 non-enzymatic functions on immune cells. However, the impact of lymphocyte-derived sCD26/DPP4 on the processing of its substrates and associated functional consequences yet remain to be addressed.

Taken together, we identified cytotoxic lymphocytes as a major cellular source of sCD26/DPP4 that is released upon degranulation. We thus provide a link between disease-associated variations in CD26/DPP4 serum levels and lymphocyte-mediated cytotoxicity. Future analyses have to answer

the question whether sCD26/DPP4 might link the cytotoxic immune response to the regulation of blood glucose levels. Moreover, the suspected defects of immune surveillance incidentally observed upon treatment with DPP4 inhibitors during diabetes mellitus type 2 therapy highlight the need for in-depth analyses of the role of sCD26/DPP4 in the effector function of cytotoxic lymphocytes.

Materials and methods

Cells

Peripheral blood mononuclear cells (PBMC) were isolated from blood specimen of healthy donors (provided by the Institute for Transfusion Medicine of the University Hospital Schleswig-Holstein Campus Kiel) by Ficoll (Merck, Darmstadt, Germany) density gradient centrifugation. $CD8^+$ T cells were MACS-purified from PBMC using a $CD8^+$ T-cell isolation kit according to manufacturer's instructions (Miltenyi Biotec, Bergisch-Gladbach, Germany) and stimulated using a feeder cocktail with irradiated EBV-transformed B lymphoblastoid cells and freshly prepared allogeneic peripheral blood mononuclear cells in the presence of 0.5 µg/mL phytohemagglutinin A (PHA, Thermo Fisher Scientific, Waltham, MA, USA) and rIL-2 (100 U/mL, Novartis, Basel, Switzerland) in RPMI 1640 with 2 mM glutamine and 25 mM HEPES (Thermo Fisher Scientific) supplemented with 100 U/mL penicillin/100 µg/mL streptomycin (Thermo Fisher Scientific) and 10% heat-inactivated FBS (Thermo Fisher Scientific). After 3–4 days, dead cells were removed by Ficoll gradient centrifugation and T-cell blasts were expanded in culture medium with rIL-2 (100 U/mL). Vδ2 T cells were enriched after initial stimulation of PBMC with Zoledronate (5 µM, kindly provided by Novartis) and expansion in RPMI 1640 with supplements and rIL-2 (50 U/mL). For expansion, fresh medium and rIL-2 were added every 3–4 days. After 14 days of expansion > 95% of cells were $CD3^+$/TCR $\gamma\delta^+$. NK cells were MACS-purified using an NK-cell isolation kit (Miltenyi Biotec) according to manufacturer's instructions and expanded in NK MACS medium (Miltenyi Biotec) supplemented with 100 U/mL penicillin/100 µg/mL streptomycin, 5% AB serum (PAA Laboratories GmbH, Pasching, Austria) and rIL-2 (500 U/mL). The phenotype of cell lines was periodically checked by flow cytometry. All blood donors provided informed consent, and the study was approved by the Institutional Ethics Review Board of Kiel University Medical Faculty (D485/14). The pancreatic ductal adenocarcinoma cell line Panc89 was kindly provided by Dr. Christian Röder (Institute for Experimental Cancer Research, UKSH/CAU, Kiel) and has been extensively characterized by ultrastructural grading, immunocytochemistry and mutational status [45]. Panc89 cells were grown in RPMI-1640 medium supplemented with 10% heat-inactivated FBS, 100 U/mL penicillin and 100 µg/mL streptomycin. For passaging, adherent tumor cells were detached from flasks with 0.05% trypsin/0.02% EDTA (Thermo Fisher Scientific). Mycoplasma negativity was routinely tested by RT-PCR using the Venor® GeM Classic mycoplasma detection kit (Minerva Biolabs, Berlin, Germany).

Cell stimulation

Cells (14–20 days after stimulation) were adjusted to 1×10^6 cells per mL and 180 µL of the cell suspension were transferred to 96 well flat-bottom plates. Anti-CD3 mab OKT3 (f.c. 1 µg/mL, Cilag, Sulzbach, Germany) and cross-linking rabbit anti-mouse IgG (f.c. 1.2 µg/mL, Jackson Immunoresearch Laboratories, West Grove, PA, USA) were added in an additional 20 µL to stimulate the cells for up to 3 h. At the end of the indicated incubation period, cells were transferred to a second 96 well V-bottom plate and subjected to immunofluorescence staining for flow cytometry (see below). In addition, supernatants were harvested, cleared by centrifugation and stored at − 20 °C for the assessment of released sCD26/DPP4 by ELISA (see below). Pre-incubation with the following inhibitors and reagents was performed for 30 min at 37 °C: EGTA at 4 mM (Merck, Darmstadt, Germany), $MgCl_2$ at 4 mM (Merck) and Cycloheximide (CHX) at 1 µM (Merck).

For the analysis of sCD26/DPP4 by precipitation and Western blot, Zoledronate-expanded γδ T cells (14–20 days of expansion) were adjusted to 2×10^6 cells/mL in serum-free X-Vivo medium (Thermo Fisher Scientific) supplemented with antibiotics and IL-2 (50 U/mL) and 10 mL of the cell suspension were transferred to a 10 cm cell culture dish. TPA (12-O-tetradecanoylphorbol-13-acetate, also termed PMA, f.c. 20 ng/mL, Merck) and ionomycin (f.c. 500 ng/mL, Merck) were added to stimulate the cells for 2 h. Following stimulation, the cells were washed once with PBS and lysed in a standard NP40 lysis buffer (1% (*v*/*v*) Nonidet®P40 (Sigma-Aldrich, St. Louis, MO, USA), 20 mM Tris–buffer, pH 7.4, 150 mM NaCl, 5 mM EDTA) supplemented with protease/phosphatase inhibitors including sodium orthovanadate, sodium fluoride, sodium pyrophosphate, phenylmethylsulfonyl fluoride, and pepstatin A (all from Sigma-Aldrich). The supernatant was centrifuged twice at 3400×*g* to remove residual cells and subjected to immunoprecipitation (see below).

Co-culture of γδ T cells with Panc89 cells

A total of 6.500 Panc89 cells/well were added to 96-well flat-bottom plates and were allowed to adhere at 37 °C overnight. Thereafter, γδ T cells, 50 U/mL IL-2 and 300 nM

BrHPP were added at effector/target (E/T) ratios of 50/1, 25/1 and 5/1. The cells were incubated for 4 h at 37 °C before the supernatants were harvested, cleared by centrifugation and stored at − 20 °C for the assessment of released sCD26/DPP4 and GrzB by ELISA (see below).

Immunofluorescent staining

For the analysis of CD26/DPP4 surface expression by conventional flow cytometry, 1.8×10^5 cells were centrifuged in 96 well V-bottom plates, washed and stained with an FITC-conjugated anti-CD26/DPP4 mab (clone BA5b, BioLegend, San Diego, CA, USA). After incubation for 30 min on ice, the cells were washed twice, fixed in 1% paraformaldehyde and analyzed on a FACSCalibur flow cytometer using CellQuestTM analysis software (BD Biosciences, Franklin Lakes, NJ, USA).

For imaging flow cytometry, $1–5 \times 10^5$ cells were centrifuged in 96-well V-bottom plates, washed and stained with fluorophore-conjugated monoclonal antibodies directed against surface expressed antigens for 30 min on ice. For the staining of intracellular antigens, cells were washed again, fixed and permeabilized employing the Cytofix/Cytoperm kit (BD Biosciences) following the manufacturer's instructions. After fixation in 1% paraformaldehyde, the cells were analyzed with an ImageStream X Mark II Imaging cytometer. The following antibodies were used for fluorescent labeling of cells: Brilliant Violet 421-conjugated anti-CD3 mab (clone UCHT1, BioLegend), Brilliant Violet 421-conjugated anti-CD4 mab (clone OKT4, BioLegend), Brilliant Violet 421-conjugated anti-CD8 mab (clone RPA-T8, BioLegend), FITC-conjugated anti-CD26/DPP4 mab (clone BA5b, BioLegend), PE-conjugated anti-granzyme A mab (clone CB9, BioLegend), PE-conjugated anti-granzyme B mab (clone GB11, Thermo Fisher Scientific), PE-conjugated anti-perforin mab (clone dG9, BioLegend), PE-conjugated anti-granulysin mab (clone DH2, BioLegend), APC-conjugated anti-TCR α/β mab (clone IP26, BioLegend), APC-conjugated anti-TCR γ/δ mab (clone B1, BioLegend) and APC-conjugated anti-CD56 mab (clone 5.1H11, BioLegend). FITC-conjugated IgG2a (clone 713, Immunotools, Friesoythe, Germany), PE-conjugated IgG1 (clone 1F8, Immunotools) and PE-conjugated IgG2a (clone PPV-04, Immunotools) served as isotype controls.

Imaging flow cytometry

The ImageStream X Mark II (Merck Millipore, Burlington, MA, USA) one camera system with 351, 488, 562, 658 and 732 nm lasers was used for imaging flow cytometry. The system was calibrated using SpeedBeads (Amnis, Seattle, WA) prior to use and at least 10.000 events with an area > 12.5 μm^2 based on brightfield images per experimental or isotype control sample were acquired. Moreover, 1.000 events of single stained compensation control samples gated on appropriate signal size were acquired with both the bright field channel and the 732 nm laser turned off. Images (Brilliant Violet 421 in channel 1, FITC and in channel 2, PE in channel 3, APC and Far Red Fixable Dye in channel 5 and bright field in channel 6) were acquired at 60-fold magnification. The integrated software INSPIRE® was used for data collection as raw image files. Raw image files of a respective staining and the corresponding isotype control files were merged. Single color controls were used to calculate a spectral crosstalk matrix that was applied to each raw image file for spectral compensations in the detection channels. Analysis was performed on the compensated image files using the IDEAS® image analysis software. The bright field gradient root mean square (RMS) feature was used to gate on cells that were in focus. Bright field area versus aspect ratio features were plotted and used to gate on single cells. Cells with saturated pixels were excluded from the analysis by plotting the histogram for the Saturation Count feature (number of saturated pixels in each cell) and gating only on cells with a saturation count of 0. Analyte-positive cells were discriminated based on controls. The bright detail similarity R3 feature was used to quantify the degree of co-localization in double positive cells only.

Subcellular fractionation

Lysosome-related effector organelles were enriched from expanded human T cells as described previously [30] employing a commercial Lysosome Isolation Kit (Sigma-Aldrich). Briefly, 4×10^8 T cells were washed with cold PBS and resuspended in extraction buffer supplemented with protease inhibitors. Cells were disrupted using a tungsten-carbide ball cell homogenizer (Isobiotec, Heidelberg, Germany). Cell homogenates (whole cell lysate, WCL) were centrifuged at 3400×*g* for 10 min to pellet nuclei and remaining intact cells. The post nuclear supernatant (enriched organelles, EO) was centrifuged at 15.000×*g* for 20 min. The supernatant (cytosol, CYT) was kept for further analysis and the organelle pellet (crude lysosomal fraction, CLF) was adjusted to 19% (*v/v*) Optiprep® (Sigma) before applying it to a non-ionic, low osmotic discontinuous density gradient with 27%, 22.5%, 19%, 16%, 12%, 8% Optiprep® layers. Organelles were separated by ultracentrifugation at 150.000×*g* for 5 h. The subcellular fractions were collected from the top of the tube, washed and concentrated with homogenization buffer (250 mM sucrose, 10 mM Hepes, pH 7.3; 0.3 mM EDTA) at 20.000×*g* for 20 min. All ultracentrifugation steps were carried out at 4 °C in ultra-clear centrifugation tubes in a swing-out rotor (SW60Ti, Beckman Coulter, Krefeld, Germany).

Immunoprecipitation

For immunoprecipitation of sCD26/DPP4, NP-40 lysates or cleared culture supernatants were incubated on a rotator with 2 µg of an anti-CD26/DPP4 mab (clone 202.36, Santa Cruz Biotechnology, Dallas, TX, USA) and protein G Sepharose beads (GE Healthcare, Chicag, IL, USA) at 4 °C for at least 120 min and subjected to SDS-PAGE after three washing steps and boiling in sample buffer.

Western blot

After gel electrophoresis following standard protocols using Bis–Tris NuPAGE gels (Thermo Fisher Scientific), proteins were transferred to 0.45 µm nitrocellulose membranes (GE Healthcare) and membranes were routinely blocked with bovine serum albumin (Sigma-Aldrich) in TBST (5%, *w/v*). The following antibodies were used for Western blot analyses: anti-CD26/DPP4 mab clone D6D8K (Abcam, Cambridge, UK), anti-Granzyme B mab clone 2C/F5 (BD Biosciences), anti-CD107a/Lamp1 mab clone 25 (BD Biosciences) and anti-GAPDH mab clone 6C5 (Santa Cruz Biotechnology, Santa Cruz, CA, USA). ECL reagents (GE Healthcare) were used for chemiluminescence detection using Hyper Film (GE Healthcare).

Enzyme-linked immunosorbent assay (ELISA)

Levels of soluble sCD26/DPP4 and granzyme B in cell-free supernatants were determined by sandwich enzyme-linked immunosorbent assays (ELISA) from Bio-Techne following the manufacturer's instructions. In individual experiments, supernatants were additionally cleared by ultracentrifugation at 100.000×*g* for 1 h prior ELISA.

DPP4 protease activity assay

DPP4 protease activity in cell- and serum-free supernatants was assessed employing a commercial fluorogenic activity assay kit (Sigma-Aldrich) following the manufacturer's instructions.

Statistical analysis

We used Graph Pad Prism 6 to perform statistical analysis. Two-tailed Mann–Whitney *U* test was used to compare the data between two groups without adjusting for multiple testing. A two-tailed *p* value of 0.10 was considered statistically significant for experiments with three samples. A two-tailed *p* value of 0.05 was considered statistically significant for experiments with more than three samples.

Acknowledgements This work was supported by the Deutsche Forschungsgemeinschaft [DFG, Grant Numbers JA 610 7/1 (to OJ) and Ka 502/19-1 (to DK)]; the Medical Faculty of the University of Kiel; and the Cluster of Excellence Exc 306 'Inflammation-at-Interfaces' Cluster Lab VII. We thank Ina Martens for expert technical assistance. This work forms part of the master theses of FA and SV and the MD theses of MD and TMD.

Compliance with ethical standards

Conflict of interest The authors declare no conflict of interest.

References

1. Klemann C, Wagner L, Stephan M, von Hörsten S (2016) Cut to the chase: a review of CD26/dipeptidyl peptidase-4's (DPP4) entanglement in the immune system. Clin Exp Immunol 185:1–21. https://doi.org/10.1111/cei.12781
2. Schon E, Demuth HU, Eichmann E, Horst HJ, Korner IJ, Kopp J, Mattern T, Neubert K, Noll F, Ulmer AJ (1989) Dipeptidyl peptidase IV in human T lymphocytes. Impaired induction of interleukin 2 and gamma interferon due to specific inhibition of dipeptidyl peptidase IV. Scand J Immunol 29:127–132
3. Ohnuma K, Yamochi T, Uchiyama M, Nishibashi K, Yoshikawa N, Shimizu N, Iwata S, Tanaka H, Dang NH, Morimoto C (2004) CD26 up-regulates expression of CD86 on antigen-presenting cells by means of caveolin-1. Proc Natl Acad Sci USA 101:14186–14191. https://doi.org/10.1073/pnas.0405266101
4. Ohnuma K, Uchiyama M, Yamochi T, Nishibashi K, Hosono O, Takahashi N, Kina S, Tanaka H, Lin X, Dang NH, Morimoto C (2007) Caveolin-1 triggers T-cell activation via CD26 in association with CARMA1. J Biol Chem 282:10117–10131. https://doi.org/10.1074/jbc.M609157200
5. Ohnuma K, Uchiyama M, Hatano R, Takasawa W, Endo Y, Dang NH, Morimoto C (2009) Blockade of CD26-mediated T cell costimulation with soluble caveolin-1-Ig fusion protein induces anergy in CD4+T cells. Biochem Biophys Res Commun 386:327–332. https://doi.org/10.1016/j.bbrc.2009.06.027
6. Hatano R, Ohnuma K, Yamamoto J, Dang NH, Morimoto C (2013) CD26-mediated co-stimulation in human CD8(+) T cells provokes effector function via pro-inflammatory cytokine production. Immunology 138:165–172. https://doi.org/10.1111/imm.12028
7. Durinx C, Lambeir AM, Bosmans E, Falmagne JB, Berghmans R, Haemers A, Scharpe S, De M I (2000) Molecular characterization of dipeptidyl peptidase activity in serum: soluble CD26/dipeptidyl peptidase IV is responsible for the release of X-Pro dipeptides. Eur J Biochem 267:5608–5613 **ejb1634 [pii]**
8. Cordero OJ, Salgado FJ, Nogueira M (2009) On the origin of serum CD26 and its altered concentration in cancer patients. Cancer Immunol Immunother 58:1723–1747. https://doi.org/10.1007/s00262-009-0728-1
9. Mulvihill EE, Drucker DJ (2014) Pharmacology, physiology, and mechanisms of action of dipeptidyl peptidase-4 inhibitors. Endocr Rev 35:992–1019. https://doi.org/10.1210/er.2014-1035
10. Yazbeck R, Jaenisch SE, Abbott CA (2018) Potential disease biomarkers: dipeptidyl peptidase 4 and fibroblast activation protein. Protoplasma 255:375–386. https://doi.org/10.1007/s00709-017-1129-5

11. Rohrborn D, Wronkowitz N, Eckel J (2015) DPP4 in diabetes. Front Immunol 6:386. https://doi.org/10.3389/fimmu.2015.00386
12. Sportiello L, Rafaniello C, Scavone C, Vitale C, Rossi F, Capuano A (2016) The importance of Pharmacovigilance for the drug safety: focus on cardiovascular profile of incretin-based therapy. Int J Cardiol 202:731. https://doi.org/10.1016/j.ijcard.2015.10.002
13. Willemen MJ, Mantel-Teeuwisse AK, Straus SM, Meyboom RH, Egberts TC, Leufkens HG (2011) Use of dipeptidyl peptidase-4 inhibitors and the reporting of infections: a disproportionality analysis in the World Health Organization VigiBase. Diabetes Care 34:369–374. https://doi.org/10.2337/dc10-1771
14. Tkac I, Raz I (2017) Combined analysis of three large interventional trials with gliptins indicates increased incidence of acute pancreatitis in patients with type 2 diabetes. Diabetes Care 40:284–286. https://doi.org/10.2337/dc15-1707
15. Overbeek JA, Bakker M, van der Heijden AAWA, van Herk-Sukel MPP, Herings RMC, Nijpels G (2018) Risk of dipeptidyl peptidase-4 (DPP-4) inhibitors on site-specific cancer: a systematic review and meta-analysis. Diabetes Metab Res Rev 34:e3004. https://doi.org/10.1002/dmrr.3004
16. Abbott CA, Baker E, Sutherland GR, McCaughan GW (1994) Genomic organization, exact localization, and tissue expression of the human CD26 (dipeptidyl peptidase IV) gene. Immunogenetics 40:331–338
17. Hong WJ, Petell JK, Swank D, Sanford J, Hixson DC, Doyle D (1989) Expression of dipeptidyl peptidase IV in rat tissues is mainly regulated at the mRNA levels. Exp Cell Res 182:256–266
18. Dinjens WN, ten KJ, van der Linden EP, Wijnen JT, Khan PM, Bosman FT (1989) Distribution of adenosine deaminase complexing protein (ADCP) in human tissues. J Histochem Cytochem 37:1869–1875. https://doi.org/10.1177/37.12.2573631
19. Bailey SR, Nelson MH, Majchrzak K, Bowers JS, Wyatt MM, Smith AS, Neal LR, Shirai K, Carpenito C, June CH, Zilliox MJ, Paulos CM (2017) Human CD26(high) T cells elicit tumor immunity against multiple malignancies via enhanced migration and persistence. Nat Commun 8:1961. https://doi.org/10.1038/s41467-017-01867-9
20. Kopinska A, Krawczyk-Kulis M, Dziaczkowska-Suszek J, Bieszczad K, Jagoda K, Kyrcz-Krzemien S (2017) The importance of the number of transplanted cells with dipeptidyl peptidase-4 expression on the haematopoietic recovery and lymphocyte reconstitution in patients with multiple myeloma after autologous haematopoietic stem-cell transplantation. Hematol Oncol 35:225–231. https://doi.org/10.1002/hon.2267
21. Mulvihill EE, Varin EM, Gladanac B, Campbell JE, Ussher JR, Baggio LL, Yusta B, Ayala J, Burmeister MA, Matthews D, Bang KWA, Ayala JE, Drucker DJ (2017) Cellular sites and mechanisms linking reduction of dipeptidyl peptidase-4 activity to control of incretin hormone action and glucose homeostasis. Cell Metab 25:152–165. https://doi.org/10.1016/j.cmet.2016.10.007
22. Casrouge A, Sauer AV, da Barreira SR, Tejera-Alhambra M, Sanchez-Ramon S, ICAReB, Cancrini C, Ingersoll MA, Aiuti A, Albert ML (2018) Lymphocytes are a major source of circulating soluble dipeptidyl peptidase 4. Clin Exp Immunol 194:166–179. https://doi.org/10.1111/cei.13163
23. Schmidt H, Gelhaus C, Nebendahl M, Lettau M, Lucius R, Leippe M, Kabelitz D, Janssen O (2011) Effector granules in human T lymphocytes: the luminal proteome of secretory lysosomes from human T cells. Cell Commun Signal 9:4. https://doi.org/10.1186/1478-811X-9-4
24. Schmidt H, Gelhaus C, Nebendahl M, Lettau M, Lucius R, Leippe M, Kabelitz D, Janssen O (2011) Effector granules in human T lymphocytes: proteomic evidence for two distinct species of cytotoxic effector vesicles. J Proteome Res 10:1603–1620. https://doi.org/10.1021/pr100967v
25. Van Acker HH, Capsomidis A, Smits EL, Van Tendeloo VF (2017) CD56 in the immune system: more than a marker for cytotoxicity? Front Immunol 8:892. https://doi.org/10.3389/fimmu.2017.00892
26. Lettau M, Kabelitz D, Janssen O (2015) Lysosome-related effector vesicles in T lymphocytes and NK cells. Scand J Immunol 82:235–243. https://doi.org/10.1111/sji.12337
27. Beum PV, Lindorfer MA, Hall BE, George TC, Frost K, Morrissey PJ, Taylor RP (2006) Quantitative analysis of protein co-localization on B cells opsonized with rituximab and complement using the ImageStream multispectral imaging flow cytometer. J Immunol Methods 317:90–99. https://doi.org/10.1016/j.jim.2006.09.012
28. Lettau M, Armbrust F, Dohmen K, Drews L, Poch T, Dietz M, Kabelitz D, Janssen O (2018) Mechanistic peculiarities of activation-induced mobilization of cytotoxic effector proteins in human T cells. Int Immunol 30:215–228. https://doi.org/10.1093/intimm/dxy007
29. Dieli F, Gebbia N, Poccia F, Caccamo N, Montesano C, Fulfaro F, Arcara C, Valerio MR, Meraviglia S, Di SC, Sireci G, Salerno A (2003) Induction of gammadelta T-lymphocyte effector functions by bisphosphonate zoledronic acid in cancer patients in vivo. Blood 102:2310–2311. https://doi.org/10.1182/blood-2003-05-1655
30. Schmidt H, Gelhaus C, Lucius R, Nebendahl M, Leippe M, Janssen O (2009) Enrichment and analysis of secretory lysosomes from lymphocyte populations. BMC Immunol 10:41. https://doi.org/10.1186/1471-2172-10-41
31. Oberg HH, Peipp M, Kellner C, Sebens S, Krause S, Petrick D, Adam-Klages S, Rocken C, Becker T, Vogel I, Weisner D, Freitag-Wolf S, Gramatzki M, Kabelitz D, Wesch D (2014) Novel bispecific antibodies increase gammadelta T-cell cytotoxicity against pancreatic cancer cells. Cancer Res 74:1349–1360. https://doi.org/10.1158/0008-5472.CAN-13-0675
32. Fukui Y, Yamamoto A, Kyoden T, Kato K, Tashiro Y (1990) Quantitative immunogold localization of dipeptidyl peptidase IV (DPP IV) in rat liver cells. Cell Struct Funct 15:117–125
33. Poulsen MD, Hansen GH, Dabelsteen E, Hoyer PE, Noren O, Sjostrom H (1993) Dipeptidyl peptidase IV is sorted to the secretory granules in pancreatic islet A-cells. J Histochem Cytochem 41:81–88. https://doi.org/10.1177/41.1.8093256
34. Casey TM, Meade JL, Hewitt EW (2007) Organelle proteomics: identification of the exocytic machinery associated with the natural killer cell secretory lysosome. Mol Cell Proteomics 6:767–780. https://doi.org/10.1074/mcp.M600365-MCP200
35. Mattern T, Reich C, Duchrow M, Ansorge S, Ulmer AJ, Flad HD (1995) Antibody-induced modulation of CD26 surface expression. Immunology 84:595–600
36. Wang Z, Grigo C, Steinbeck J, von Hörsten S, Amann K, Daniel C (2014) Soluble DPP4 originates in part from bone marrow cells and not from the kidney. Peptides 57:109–117. https://doi.org/10.1016/j.peptides.2014.05.006
37. Nargis T, Kumar K, Ghosh AR, Sharma A, Rudra D, Sen D, Chakrabarti S, Mukhopadhyay S, Ganguly D, Chakrabarti P (2017) KLK5 induces shedding of DPP4 from circulatory Th17 cells in type 2 diabetes. Mol Metab 6:1529–1539. https://doi.org/10.1016/j.molmet.2017.09.004
38. Zillessen P, Celner J, Kretschmann A, Pfeifer A, Racke K, Mayer P (2016) Metabolic role of dipeptidyl peptidase 4 (DPP4) in primary human (pre)adipocytes. Sci Rep 6:23074. https://doi.org/10.1038/srep23074
39. Rohrborn D, Eckel J, Sell H (2014) Shedding of dipeptidyl peptidase 4 is mediated by metalloproteases and up-regulated by hypoxia in human adipocytes and smooth muscle cells. FEBS Lett 588:3870–3877. https://doi.org/10.1016/j.febslet.2014.08.029

40. Varin EM, Mulvihill EE, Beaudry JL, Pujadas G, Fuchs S, Tanti JF, Fazio S, Kaur K, Cao X, Baggio LL, Matthews D, Campbell JE, Drucker DJ (2018) Circulating levels of soluble dipeptidyl peptidase-4 are dissociated from inflammation and induced by enzymatic DPP4 inhibition. Cell Metab. https://doi.org/10.1016/j.cmet.2018.10.001
41. Ghorpade DS, Ozcan L, Zheng Z, Nicoloro SM, Shen Y, Chen E, Bluher M, Czech MP, Tabas I (2018) Hepatocyte-secreted DPP4 in obesity promotes adipose inflammation and insulin resistance. Nature 555:673–677. https://doi.org/10.1038/nature26138
42. Shioda T, Kato H, Ohnishi Y, Tashiro K, Ikegawa M, Nakayama EE, Hu H, Kato A, Sakai Y, Liu H, Honjo T, Nomoto A, Iwamoto A, Morimoto C, Nagai Y (1998) Anti-HIV-1 and chemotactic activities of human stromal cell-derived factor 1alpha (SDF-1alpha) and SDF-1beta are abolished by CD26/dipeptidyl peptidase IV-mediated cleavage. Proc Natl Acad Sci USA 95:6331–6336
43. Crump MP, Gong JH, Loetscher P, Rajarathnam K, Amara A, Arenzana-Seisdedos F, Virelizier JL, Baggiolini M, Sykes BD, Clark-Lewis I (1997) Solution structure and basis for functional activity of stromal cell-derived factor-1; dissociation of CXCR1 activation from binding and inhibition of HIV-1. EMBO J 16:6996–7007. https://doi.org/10.1093/emboj/16.23.6996
44. Decalf J, Tarbell KV, Casrouge A, Price JD, Linder G, Mottez E, Sultanik P, Mallet V, Pol S, Duffy D, Albert ML (2016) Inhibition of DPP4 activity in humans establishes its in vivo role in CXCL10 post-translational modification: prospective placebo-controlled clinical studies. EMBO Mol Med 8:679–683. https://doi.org/10.15252/emmm.201506145
45. Sipos B, Moser S, Kalthoff H, Torok V, Lohr M, Kloppel G (2003) A comprehensive characterization of pancreatic ductal carcinoma cell lines: towards the establishment of an in vitro research platform. Virchows Arch 442:444–452. https://doi.org/10.1007/s00428-003-0784-4